Discrete-to-continuum models of pre-stressed cytoskeletal filament networks

Supplementary Material

J. Köry[1], N. A. Hill[1], X. Luo[1] and P. S. Stewart[1]

[1]School of Mathematics and Statistics, University of Glasgow, Mathematics and Statistics Building, University Place, Glasgow G12 8QQ, UK

April 3, 2024

This Supplementary Material is organized as follows. Section S1 summarizes notation adopted throughout this article. Model parameters together with their default values are listed in Section S2. Section S3 contains detailed derivations pertaining to the discrete model and Section S4 to the upscaling and the resulting continuum model. Finally, Section S5 presents calculations relating to the small-deformations and small-bead limits, including that of the net force acting on the bead.

S1 Summary of notation

Below we list notation adopted in this work, stating the symbols and their definitions. We note that this table is not exhaustive but with its help one can easily deduce all notation adopted in this work. For example, the mesh spacing representative of the cytoskeleton ε_c is obtained by adding subscript c to the mesh spacing ε.

General

FS	Abbreviation for filament segment
CL	Abbreviation for crosslink
$\sim$	Dimensional variable (above the symbol)
i, j	Indices of the discrete network (as subscript)
kl	Indices of tensors attaining value 1 or 2 for the two spatial dimensions (as subscript)
c	Value representative of the cytoskeleton (as subscript)
I/O	Pertaining to inner/outer region (as superscript)

Variables and Functions

$\boldsymbol{X} = (X, Y)$	Initial configuration variables
$\boldsymbol{x} = (x, y)$	Deformed configuration variables
(u, v)	Components of the displacement field
$(\hat{x}, \hat{y})$	Small-deformations variables
$\left(\bar{X}, \bar{Y}\right)$	Initial configuration variables rescaled to the bead boundary region
$\bar{Z}$	Stretched $\bar{Y}$ coordinate
(μ, ν)	Elliptical coordinates
$\tilde{r}$	End-to-end distance (straight-line distance between two ends of a filament segment)
r	End-to-end distance normalized with respect to the stress-free contour length

f	Axial force in a filament segment (scales with N)
$\mathcal{F}$	Axial force in a filament segment ($N = N_c$)
e	Energy stored in a filament segment (scales with N)
$\mathcal{E}$	Energy stored in a filament segment ($N = N_c$)
φ	Polar angle

Parameters of the initial configuration

$\tilde{D}$	Domain length
N	Number of filament segments belonging to one filament
$\tilde{R}$	Initial mesh spacing
ε	Dimensionless initial mesh spacing
$\tilde{L}$	Stress-free contour length of a filament
$\tilde{\Lambda}$	Stress-free contour length of a filament segment
ξ	Initial mesh spacing normalized with respect to the stress-free contour length
f_p	Force in a filament segment due to pre-stress (scales with N)
$\mathcal{F}_p$	Force in a filament segment due to pre-stress ($N = N_c$)
ω	Dimensionless parameter of the small-deformations problem
$\tilde{\sigma}_p$	Macroscale pre-stress
a	Bead radius

Material properties of the filaments

$\tilde{Y}$	Young's modulus of a filament
$\tilde{b}$	Radius of a filament
$\tilde{k}_B$	Boltzmann constant
$\tilde{T}$	Absolute temperature
$\tilde{\Lambda}_p$	Persistence length of a filament
$\tilde{\mathcal{F}}_{\text{entropic}}$	Entropic force
$\tilde{\mathcal{F}}_{\text{enthalpic}}$	Enthalpic force
$\mathcal{T}_1$	Ratio of the entropic force to the enthalpic force
$\mathcal{T}_2$	One half of the ratio of the persistence length to the initial end-to-end distance

Deformation

φ_*	Pulling angle
R_b	Magnitude of the bead displacement
F_b	Magnitude of the net force acting on the bead
$\mathcal{K}$	Scalar measure of network stiffness
$\hat{\boldsymbol{r}}_{i\pm\frac{1}{2},j}/\hat{\boldsymbol{r}}_{i,j\pm\frac{1}{2}}$	Unit vectors pointing in the directions of filament segments adjacent to node (i,j)
$l_{i\pm\frac{1}{2},j}/l_{i,j\pm\frac{1}{2}}$	Deformed lengths of the filament segments
$\boldsymbol{I}$	Identity tensor
$\boldsymbol{F}$	Deformation gradient tensor

$\boldsymbol{C}$	Right Cauchy-Green deformation tensor
$I_{4/6}(\boldsymbol{C})$	Invariants of the right Cauchy-Green deformation tensor
$\boldsymbol{S}$	Nominal stress tensor
W	Strain energy density

S2 Model parameters

S2.1 Summary of the dimensional and dimensionless models

The discrete model is only representative of a cytoskeletal mesh with spacing $\tilde{R}_c$ provided one takes $N = N_c = 1/\varepsilon_c = \tilde{D}/\tilde{R}_c$ - increasing N only facilitates convergence to the continuum model. Subject to the microscale constitutive law (3), the dimensional model is then governed by ten parameters - three parameters describing the initial geometry with the bead ($\tilde{D}$, $\tilde{R}_c$ and $\tilde{a}$), four parameters describing mechanical properties of the filaments under consideration ($\tilde{Y}$, $\tilde{b}_c$, $\tilde{\Lambda}_p$ and $\tilde{\mathcal{F}}_p$), two parameters governing the bead displacement ($\tilde{R}_b$ and φ_*) and temperature $\tilde{T}$. Remaining parameters can be deduced from these. Note in particular that the stress-free contour length $\tilde{\Lambda}_c(\tilde{\mathcal{F}}_p)$ can be found numerically upon substituting $\tilde{b} = \tilde{b}_c$, $\tilde{r} = \tilde{R}_c$ and $\tilde{f} = \tilde{\mathcal{F}}_p$ (provided $N = N_c$) into (3); alternatively one can use an explicit approximation (S15) derived in Section S3.3.

Subject to the microscale constitutive law (5), the dimensionless model (for $N = 1/\varepsilon_c$) is governed by 7 parameters - ε_c, a, $\mathcal{T}_1$, $\mathcal{T}_2$, $\mathcal{F}_p$, R_b and φ_* - and ξ must be found by numerically solving (7). Alternatively, one can impose the explicit approximations (9) (vimentin) or (S13) (actin; ξ is the given by (S12)) for the microscale constitutive law, in which case the dimensionless model ($N = 1/\varepsilon_c$) needs 5 parameters for both actin and vimentin - ε_c, a, $\mathcal{F}_p$, R_b and φ_* - and actin requires one more parameter ($\mathcal{T}_2$) for full specification. Recall that in each of the above cases, it is assumed that filaments cannot withstand any compressive loads.

S2.2 Default dimensional parameters

Recall the default values $\tilde{D} = 5\mu$m, $\tilde{R}_c = 0.05\mu$m, $N = (N_c =)100$ (estimated in Section 2.1), $\varphi_* = \pi/6$ and $0 \leq \tilde{R}_b \leq \tilde{R}_c$ (Section 4). We further use as default values $\tilde{T} = 300$ K for the absolute temperature and $\tilde{a} = 0.25$ μm for the bead radius [7]. The standard value of the Boltzmann constant is $\tilde{k}_B \approx 1.38 \times 10^{-23}\text{m}^2\text{kg s}^{-2}\text{K}^{-1}$.

Mechanical behaviour of actin filaments subject to tension has been widely studied experimentally. The microscale constitutive law (3) has been shown to be equivalent to another constitutive model which in turn reproduced the experimental data well [2, 6]. The following estimates for material parameters from (3) pertain to actin filaments *in vivo*: $\tilde{Y} = 2$ GPa, $\tilde{\Lambda}_p = 17\mu$m and $\tilde{b} = 3.5$ nm [8].

Even though vimentin has only gained significant attention from the scientific community relatively recently, much is already known about its tensile behaviour. Using atomistic simulations, three distinct regimes in force extension diagram of single vimentin dimer under tension were uncovered and the underlying changes in its molecular structure identified [10]. Tensile behaviour of single vimentin filaments was measured [1], confirming three distinct regimes reported previously [10], and showing good agreement between optical trap and atomic force microscopy experiments. Unfortunately, it is very unclear how these results could be translated to vimentin FSs of various contour lengths. For simplicity, we thus assume that a tensile response of a single vimentin FS can be modelled using Equation (3) with an appropriate choice of model parameters. Vimentin filaments are about 10 nm in diameter ($\tilde{b}_c = 5$ nm) and their Young's modulus was measured to be about $\tilde{Y} = 0.9$ GPa [5]. The persistence length of vimentin is approximately $\tilde{\Lambda}_p = 1\mu$m [8].

To allow as large deformations as possible without breaking the actin filaments, we take the tensile strength $\tilde{\mathcal{F}}_{\max}$ of actin to be the upper bound of the values found in the literature, i.e. 600 pN [13], and the value 8 nN provides us with a lower bound for the tensile strength of vimentin [1]. The only unknown parameter is then the value of the force due to pre-stress $\tilde{\mathcal{F}}_p$. As discussed in the main body of this paper, we have not managed to find any estimate for microscale force due to pre-stress (and, equivalently, pre-stretch ξ or stress-free contour length $\tilde{\Lambda}$ values) representative of cells *in vivo*. Therefore, $\tilde{\mathcal{F}}_p$ will here be considered a free parameter, with the default value equal to one half of the tensile strength estimates from above.

For completeness we also list the default values for the mechanical parameters of the dimensionless model to be

$$\mathcal{T}_1^{\text{actin}} \approx 1 \times 10^{-9} \qquad \mathcal{T}_2^{\text{actin}} \approx 170 \qquad \mathcal{T}_1^{\text{vimentin}} \approx 1.9 \times 10^{-8} \qquad \mathcal{T}_2^{\text{vimentin}} \approx 10.$$

Table S1 lists key model parameters together with their default values.

Table S1: Default values of discrete model parameters representative of cytoskeleton ($N = 1/\varepsilon_c = 100$). Note that whenever applicable, the default value is stated for vimentin with the value for actin in parantheses.

Parameter	Symbol	Default value	Units	Source
Cell region size	$\tilde{D}$	5	μm	biologically plausible
Inter-crosslink distance	$\tilde{R}_c$	0.05	μm	[7]
# of FSs per filament	N_c	100	-	$\tilde{D}/\tilde{R}_c$
Absolute temperature	$\tilde{T}$	300	K	*in vivo* (rounded)
Bead radius	$\tilde{a}$	0.25	μm	[7]
Bead displacement - maximum magnitude	$\tilde{R}_b$	0.05	μm	$\tilde{R}_b = \tilde{R}_c$
Bead displacement - angle	φ_*	$\pi/6$	-	generic case
Young's modulus	$\tilde{Y}$	0.9 (2.0)	GPa	[5, 8]
Filament radius	$\tilde{b}_c$	0.005 (0.0035)	μm	[5, 8]
Persistence length	$\tilde{\Lambda}_p$	1.0 (17.0)	μm	[5, 8]
Tensile strength	$\tilde{\mathcal{F}}_{\max}$	8.0 (0.6)	nN	Supplementary Section S2
Force due to pre-stress	$\tilde{\mathcal{F}}_p$	4.0 (0.3)	nN	Supplementary Section S2

S3 Discrete model

S3.1 Stored elastic energy in undeformed and deformed configurations

The total (elastic) energy of the discrete network, denoted $\tilde{e}_T$ (introducing subscript T for total), is the sum of contributions due to axial filament stretching. First let us note that the microscale constitutive law (3) is parameterized by the stress-free contour length $\tilde{\Lambda}$ which in turn scales as $O(1/N)$ in the $N \to \infty$ limit. Therefore, we simply write $\tilde{f} = \tilde{f}(\tilde{r}/\tilde{\Lambda}; N)$. We then express the elastic energy stored in an individual FS for general N as

$$\tilde{e}(r; N) = \int_{\tilde{R}_{sf}}^{r\tilde{\Lambda}} \tilde{f}\left(\frac{\tilde{s}}{\tilde{\Lambda}}; N\right) d\tilde{s}, \tag{S1}$$

where $\tilde{R}_{sf}$ denotes the stress-free end-to-end distance. Defining the deformed lengths of the FSs between neighbouring CLs as

$$\tilde{l}_{i\pm\frac{1}{2},j} = \sqrt{(\tilde{x}_{i\pm1,j} - \tilde{x}_{i,j})^2 + (\tilde{y}_{i\pm1,j} - \tilde{y}_{i,j})^2} \qquad \tilde{l}_{i,j\pm\frac{1}{2}} = \sqrt{(\tilde{x}_{i,j\pm1} - \tilde{x}_{i,j})^2 + (\tilde{y}_{i,j\pm1} - \tilde{y}_{i,j})^2}, \tag{S2}$$

where the usage of the index $\pm\frac{1}{2}$ arises naturally between any two neighbouring CLs, the total energy $\tilde{e}_T$ can be obtained by summing up these energies for all FSs, i.e.

$$\begin{aligned}\tilde{e}_T = &\sum_{i=-N/2+1}^{N/2-1} \sum_{j=-N/2+1}^{N/2-1} \left[\tilde{e}\left(\frac{\tilde{l}_{i-\frac{1}{2},j}}{\tilde{\Lambda}}; N\right) + \tilde{e}\left(\frac{\tilde{l}_{i,j-\frac{1}{2}}}{\tilde{\Lambda}}; N\right)\right] + \\ &\sum_{j=-N/2+1}^{N/2-1} \tilde{e}\left(\frac{\tilde{l}_{\frac{N}{2}-\frac{1}{2},j}}{\tilde{\Lambda}}; N\right) + \sum_{i=-N/2+1}^{N/2-1} \tilde{e}\left(\frac{\tilde{l}_{i,\frac{N}{2}-\frac{1}{2}}}{\tilde{\Lambda}}; N\right).\end{aligned} \tag{S3}$$

We assume no slippage of CLs along the filaments so that the stress-free contour lengths of every FS in the undeformed and the deformed configurations are equal to $\tilde{\Lambda}$. Following Section S3.2, we can write the axial forces as $\tilde{f}(r; N) = N_c\tilde{\mathcal{F}}(r)/N$ and express the elastic energy stored in a single FS at the undeformed end-to-end distance $\tilde{R}$ as

$$\tilde{e}(\xi; N) = \int_{\tilde{R}_{sf}}^{\tilde{R}} \frac{N_c}{N}\tilde{\mathcal{F}}\left(\frac{\tilde{s}}{\tilde{\Lambda}}\right) d\tilde{s}, \tag{S4}$$

where ξ is defined in (2) and we have

$$\tilde{e}\left(\frac{\tilde{r}}{\tilde{\Lambda}}; N\right) = \int_{\tilde{R}_{sf}}^{\tilde{r}} \frac{N_c}{N}\tilde{\mathcal{F}}\left(\frac{\tilde{s}}{\tilde{\Lambda}}\right) d\tilde{s} = \tilde{e}(\xi, N) + \int_{\tilde{R}}^{\tilde{r}} \frac{N_c}{N}\tilde{\mathcal{F}}\left(\frac{\tilde{s}}{\tilde{\Lambda}}\right) d\tilde{s}. \tag{S5}$$

To derive the strain energy density in Section S4, it is also useful to introduce the elastically stored energy at an arbitrary CL (i,j) as

$$\tilde{e}_{i,j}(N) = \frac{1}{2}\left(\tilde{e}\left(\frac{\tilde{l}_{i-\frac{1}{2},j}}{\tilde{\Lambda}},N\right)+\tilde{e}\left(\frac{\tilde{l}_{i+\frac{1}{2},j}}{\tilde{\Lambda}},N\right)+\tilde{e}\left(\frac{\tilde{l}_{i,j-\frac{1}{2}}}{\tilde{\Lambda}},N\right)+\tilde{e}\left(\frac{\tilde{l}_{i,j+\frac{1}{2}}}{\tilde{\Lambda}},N\right)\right), \tag{S6}$$

where the factor $1/2$ accounts for the fact that the tensile energy stored in any FS corresponds to two CLs rather than just one. We further define $\tilde{D}_{sf} = N\tilde{R}_{sf}$. For any $r = \tilde{r}/\tilde{\Lambda}$ we can then using integration by substitution $(\tilde{s}/\tilde{\Lambda} = N\tilde{s}/\tilde{L} = t)$ write

$$\tilde{e}(r,N) = \frac{N_c}{N}\int_{\tilde{R}_{sf}}^{\tilde{\Lambda}r}\tilde{\mathcal{F}}\left(\frac{\tilde{s}}{\tilde{\Lambda}}\right)d\tilde{s} = \frac{\tilde{L}N_c}{N^2}\int_{\tilde{D}_{sf}/\tilde{L}}^{r}\tilde{\mathcal{F}}(t)dt = \left(\frac{N_c}{N}\right)^2\tilde{\mathcal{E}}(r), \tag{S7}$$

which defines the energy $\tilde{\mathcal{E}}(r)$ stored in a FS in a situation representative of cytoskeleton $(N = N_c)$. Defining $\xi_{sf} = \tilde{D}_{sf}/\tilde{L}$, this can be split into the energy due to pre-stress $\tilde{\mathcal{E}}_P$ and that supplied with the deformation $\tilde{\mathcal{E}}_D$ as

$$\tilde{\mathcal{E}}(r) = \frac{\tilde{D}}{\xi N_c}\int_{\xi_{sf}}^{\xi}\tilde{\mathcal{F}}(t)dt + \frac{\tilde{D}}{\xi N_c}\int_{\xi}^{r}\tilde{\mathcal{F}}(t)dt = \tilde{\mathcal{E}}_P + \tilde{\mathcal{E}}_D(r). \tag{S8}$$

S3.2 Decreasing the mesh spacing

S3.2.1 Scaling geometric parameters with N

In Section 3 we upscale the discrete force balance into a continuum problem as $N \to \infty$ $(\tilde{\Lambda}/\tilde{L} \to 0)$. For the continuum limit to be a good approximation of the discrete model at the baseline setup representative of the cytoskeleton (i.e. using $N = N_c = 100$; for default values of all parameters see Section S2), we need to ensure that all model parameters are appropriately scaled as $N \to \infty$. As N increases we have $\tilde{R} = N_c/N \times \tilde{R}_c$ and $\tilde{\Lambda} = N_c/N \times \tilde{\Lambda}_c$ where $\tilde{R}_c$ and $\tilde{\Lambda}_c$ are representative of the cytoskeleton. Note that the total length of the network increases without bounds as $N \to \infty$. Assuming constant density for the material of the filament, the total mass is a constant multiple of the total volume $2(N-1)\tilde{L}\pi\tilde{b}^2$ and to keep this $O(1)$ as $N \to \infty$, we assume that $\tilde{b} = \tilde{b}_c\sqrt{N_c/N}$ where $\tilde{b}_c$ is a representative radius of the filament.

S3.2.2 Scaling forces (including those due to pre-stress) with N

Next we need to ensure that we get $O(1)$ tensile pre-stress in the $N \to \infty$ limit. Substituting the above scalings into (3) and switching to $\varepsilon_c = 1/N_c$, we get in the undeformed configuration

$$\frac{\tilde{D}}{\tilde{L}} = \left(1+\frac{N\varepsilon_c\tilde{f}_p}{\pi\tilde{Y}\tilde{b}_c^2}\right)\left(1-\sqrt{\frac{\tilde{k}_B\tilde{T}}{\pi\tilde{\Lambda}_p\left(\tilde{f}_p+\frac{\pi^2\tilde{k}_B\tilde{T}\tilde{\Lambda}_pN^2}{\tilde{L}^2}\right)}}\right). \tag{S9}$$

Using a dimensionless force due to pre-stress $f_p = \tilde{f}_p/(\pi\tilde{Y}\tilde{b}_c^2)$ (as per Section 2.6), equation (S9) becomes

$$\frac{\tilde{D}}{\tilde{L}} = (1+\varepsilon_cNf_p)\left(1-\sqrt{\frac{\tilde{k}_B\tilde{T}}{\pi\tilde{\Lambda}_p\left(\pi\tilde{Y}\tilde{b}_c^2f_p+\frac{\pi^2\tilde{k}_B\tilde{T}\tilde{\Lambda}_pN^2}{\tilde{L}^2}\right)}}\right). \tag{S10}$$

Deriving an explicit relationship for $f_p(N)$ would be cumbersome and the situation is further complicated by the fact that $\tilde{L}$ depends on f_p. However, in order to keep the right-hand side of (S10) $O(1)$ in $N \to \infty$ limit, f_p must scale as $1/N$ for large N. We thus get $f_p(N) = \mathcal{F}_p/(\varepsilon_cN)$ with $\mathcal{F}_p = O(1)$, which ensures that the total elastic energy stored in the pre-stressed domain stays $O(1)$ as $N \to \infty$ and we arrive at a finite (and non-zero) pre-stress in the continuum limit.

Similarly, we must have $f(r;N) = \mathcal{F}(r)/(\varepsilon_cN)$. To demonstrate the central idea behind this scaling, resulting force distributions for $N = 10$ and 20 (and otherwise default parameters for vimentin, as described in Section S2) are shown in Figure S1. Notice how the colorbar ranges vary with increasing N, which reflects the force scaling. In other words, for the discrete simulations to converge onto an $O(1)$ force response in the continuum $(N \to \infty)$ limit, forces must scale as $1/N$ and these forces are thus in physiologically realistic range only for $N = N_c$.

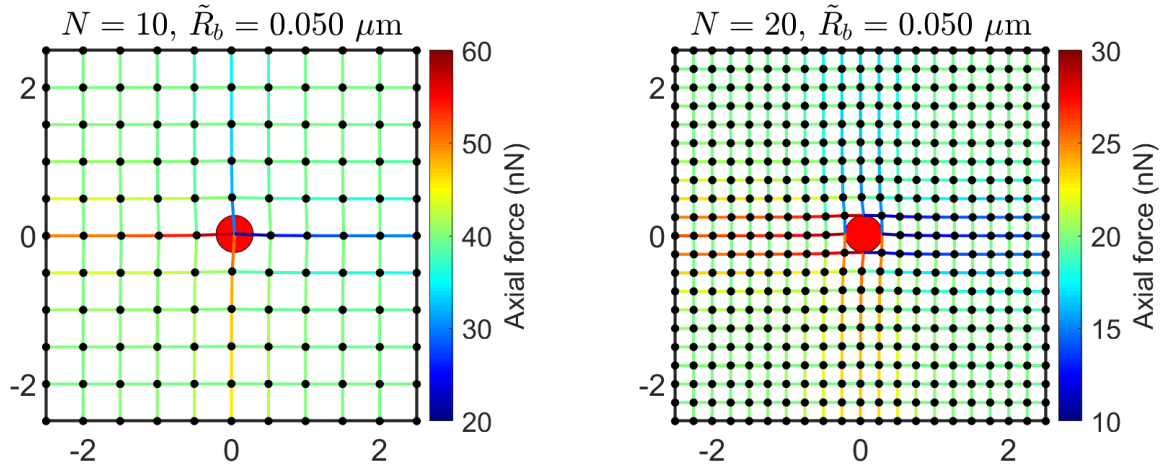

(a) $N = 10$ (b) $N = 20$

Figure S1: The solution profiles for (a) $N = 10$ and (b) $N = 20$ using default model parameters for vimentin. Note that due to the smallness of N we show profiles in full domains (not only in the vicinity of the bead as we did in the main body) and that the indicated lengths are in microns.

S3.3 Implicit and explicit microscale constitutive laws for vimentin and actin

S3.3.1 Explicit microscale constitutive laws for fixed N

We observe that $\mathcal{T}_1$ is very small for considered filaments - $\mathcal{T}_1 \approx 1.0 \times 10^{-9}$ for actin and $\mathcal{T}_1 \approx 1.9 \times 10^{-8}$ for vimentin. Substituting $\mathcal{T}_1 \ll 1$ into (7) we get (8) which provides an explicit relationship between the force due to pre-stress and pre-stretch. While this formula provides a good approximation to the implicit formula (7) for vimentin (provided the pre-stress is not too small), a non-negligible gap exists in the approximation for actin - see Figure S2. Similarly, when we plot the microscale constitutive law (5) (using ξ corresponding to the default pre-stress as found numerically from (7)) and compare it with the $\mathcal{T}_1 = 0$ approximation (9), we again observe good agreement for vimentin but a clear gap for actin (see Figure S3). The gaps for actin can be explained

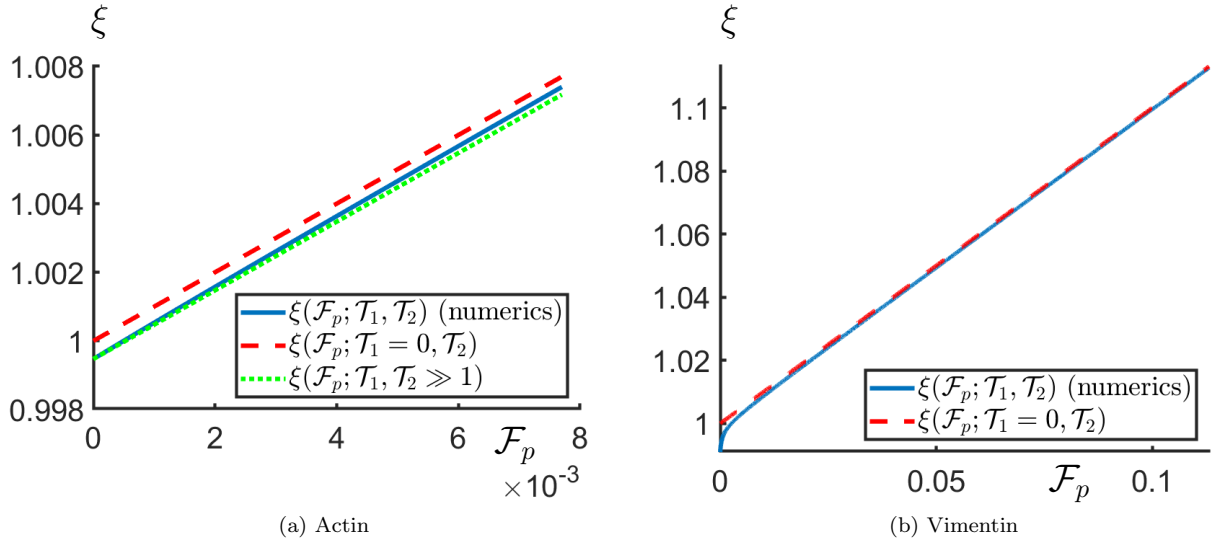

(a) Actin (b) Vimentin

Figure S2: Numerically computed $\xi(\mathcal{F}_p;\mathcal{T}_1,\mathcal{T}_2)$ (solid blue) as compared with its $\mathcal{T}_1 = 0$ approximation (dashed red) for (a) actin and (b) vimentin. The green dotted line in Figure (a) presents the approximation (S12) valid for actin.

by a combination of considered force range (the maximum considered value of $\mathcal{F}$ is small for actin compared to vimentin, due to the small tensile strength of the former) and the size of $\mathcal{T}_2$ (≈ 170 for actin, which means that the spacing between neighbouring CLs is much shorter than the persistence length of actin). Having noticed the largeness of $\mathcal{T}_2$ we (assume $\mathcal{T}_1 = O(1)$ and) substitute the ansatz

$$\xi(\mathcal{F}_p;\mathcal{T}_1,\mathcal{T}_2,\varepsilon_c,N) = \xi_0(\mathcal{F}_p;\mathcal{T}_1,\varepsilon_c,N) + \frac{1}{\mathcal{T}_2}\xi_1(\mathcal{F}_p;\mathcal{T}_1,\varepsilon_c,N) + O(\mathcal{T}_2^{-2}) \tag{S11}$$

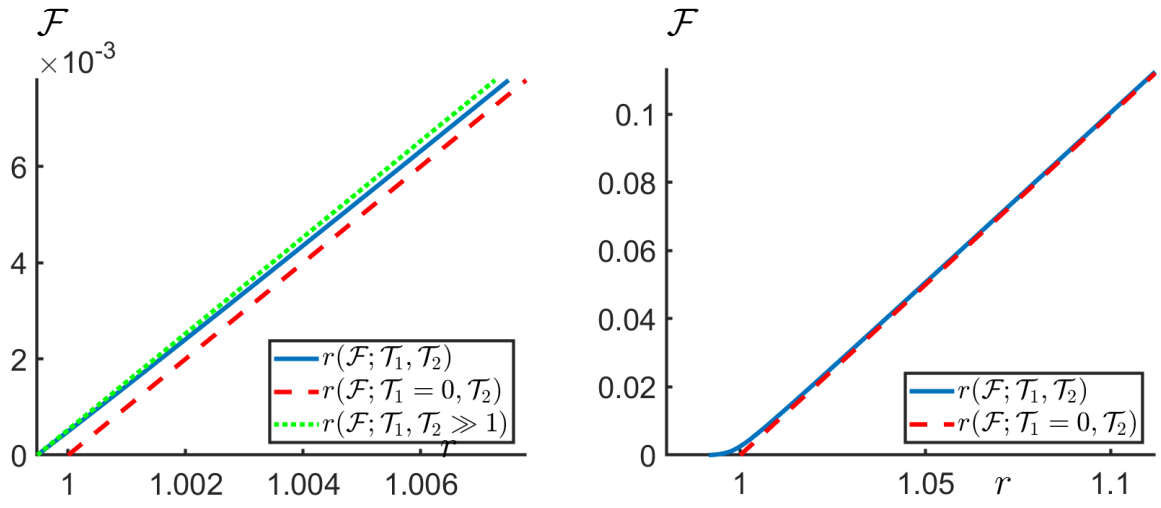

(a) Actin (b) Vimentin

Figure S3: $r(\mathcal{F};\mathcal{T}_1,\mathcal{T}_2)$ from (7) using numerically calculated ξ corresponding to default pre-stress (solid blue) as compared with its $\mathcal{T}_1=0$ approximation (dashed red) for (a) actin and (b) vimentin. The green dotted line in Figure (a) presents the approximation (S13) valid for actin.

into (7) and get

$$\xi_0+\frac{1}{\mathcal{T}_2}\xi_1+O(\mathcal{T}_2^{-2})=(1+\mathcal{F}_p)\left(1-\sqrt{\frac{\mathcal{T}_1}{\mathcal{F}_p/(\varepsilon_c N)+4\pi^3\left(\varepsilon_c N\mathcal{T}_2\right)^2\mathcal{T}_1\left(\xi_0^2+O(\sqrt{\mathcal{T}_2^{-1}})\right)}}\right).$$

At the leading order in $\mathcal{T}_2$ ($O(1)$) we again get

$$\xi_0=1+\mathcal{F}_p$$

and at $O(\mathcal{T}_2^{-1})$ we conclude

$$\xi_1=-\frac{1+\mathcal{F}_p}{2\pi^{3/2}\varepsilon_c N\xi_0^2}=-\frac{1}{2\pi^{3/2}\varepsilon_c N\left(1+\mathcal{F}_p\right)}.$$

Retaining the first two terms, the approximation reads

$$\xi=1+\mathcal{F}_p-\frac{1}{\mathcal{T}_2}\frac{1}{2\left(1+\mathcal{F}_p\right)\pi^{3/2}\varepsilon_c N}. \tag{S12}$$

For actin, this provides a good approximation (without a significant gap) to (7), as shown in Figure S2a. Similarly, we can expand (5) for $\mathcal{T}_2\gg 1$ and retaining $O(\mathcal{T}_2^{-1})$ terms we get

$$r=(1+\mathcal{F})\left(1-\frac{1}{2\pi^{3/2}\varepsilon_c N\xi\mathcal{T}_2}\right). \tag{S13}$$

Using the approximation for ξ from (S12) in (S13), we again recover an excellent approximation without a gap, see Figure S3a.

Redimensionalized microscale constitutive laws For the sake of completeness, we also state the approximate microscale constitutive laws in their dimensional forms (dimensionalizing both the force and the end-to-end distance). For vimentin, dimensionless microscale constitutive law (9) can be redimensionalized using (8) to give an expression in terms of the dimensional parameters of the approximate model (and N) which reads

$$\tilde{f}=\max\left\{0,\frac{\pi\tilde{Y}\tilde{b}_c^2}{\tilde{R}_c}\left[\left(1+\frac{\tilde{\mathcal{F}}_p}{\pi\tilde{Y}\tilde{b}_c^2}\right)\tilde{r}-\frac{\tilde{D}}{N}\right]\right\}. \tag{S14}$$

From (S12), we can deduce for actin

$$\tilde{\Lambda}=\frac{\tilde{R}}{1+\mathcal{F}_p-\frac{1}{\mathcal{T}_2}\frac{1}{2\left(1+\mathcal{F}_p\right)\pi^{3/2}\varepsilon_c N}} \tag{S15}$$

and eventually conclude from (S13) the redimensionalized microscale constitutive law in the form

$$\tilde{f} = \max\left\{0, \frac{\pi\tilde{Y}\tilde{b}_c^2}{\tilde{R}_c}\left[\frac{\xi}{1-\dfrac{\tilde{D}}{\pi^{3/2}\xi N\tilde{\Lambda}_p}}\tilde{r} - \frac{\tilde{D}}{N}\right]\right\}, \tag{S16}$$

where ξ is given in (S12).

S3.3.2 Scaling of ξ with N for fixed $\mathcal{F}_p$

We observed in Section S3.2.2 that the force due to pre-stress must scale as $f_p(N) = \mathcal{F}_p/(\varepsilon_c N)$, with $\mathcal{F}_p = O(1)$. In order to study how ξ scales with N and determine whether this scaling is consistent for both the implicit model and the explicit approximations, we fix all parameters at their default value for both actin and vimentin (including $\mathcal{F}_p$; see Section S2) and find the root ξ of (7) as function of N numerically. The log-plots in Figure S4 show that while ξ has not yet converged to its $N \to \infty$ limit $1 + \mathcal{F}_p$ for $N = 1/\varepsilon_c = 100$ (used as default throughout this work and indicated by vertical black lines in the figure), the dependence is very weak for both actin and vimentin. Moreover, (S12) provides a good approximation for $\xi(N)$ near $N = 1/\varepsilon_c = 100$ for actin (see dotted green curve in Figure S4a).

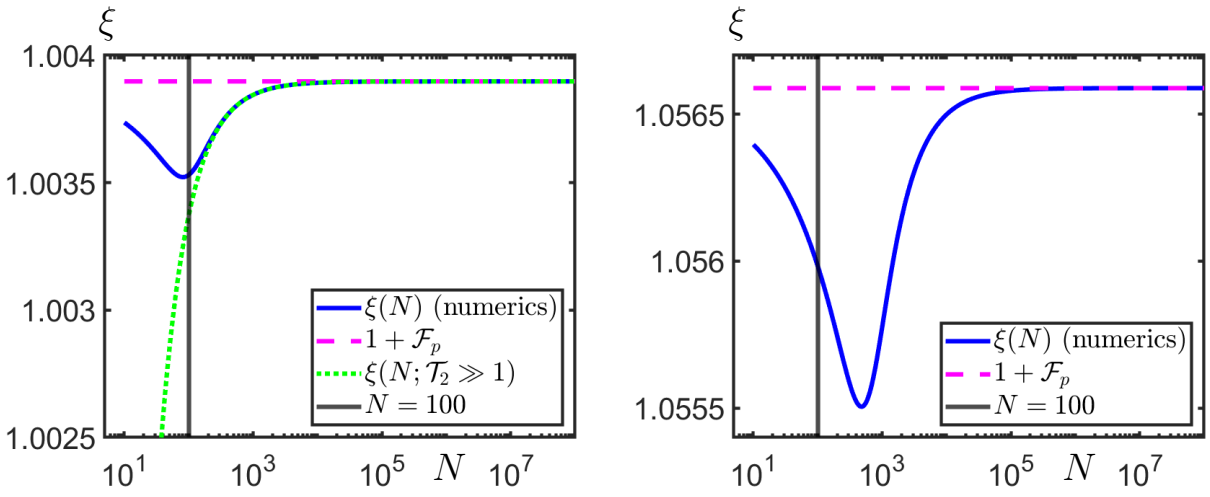

(a) Actin (b) Vimentin

Figure S4: As $N \to \infty$, for default model parameters (including $\mathcal{F}_p$) the numerically computed ξ (solid blue) converges to $1 + \mathcal{F}_p$ (dashed magenta) for both actin (a) and vimentin (b). Even though the convergence is not yet attained at $N = 1/\varepsilon_c = 100$, the dependence on N is weak. The green dotted curve in panel (a) corresponds to the approximation (S12).

S3.4 Discrete model simulations for actin

We simulated the discrete model for actin using the microscale constitutive law (S16) with ξ given by (S12). As in the main body, we plot the steady-state solutions in the vicinity of the bead. For bead displacements $\tilde{R}_b$ as

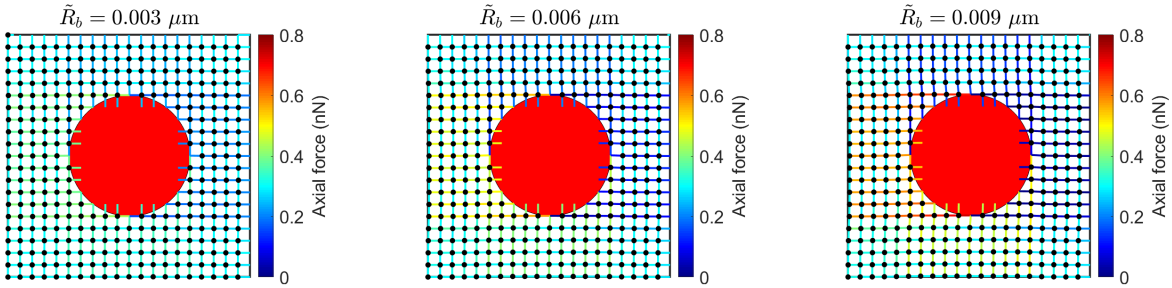

Figure S5: Steady-state solutions using default actin parameters with $N = 1/\varepsilon_c = 100$ for increasing $\tilde{R}_b$ (zoomed-in onto the bead).

small as (roughly) one tenth of the mesh size ($\tilde{R} = 0.05\mu$m), actin FSs start experiencing tensile forces beyond the upper limit of their tensile strength, 600 pN (see Figure S5). In particular, FSs in the wake of the bead motion whose undeformed orientation has a significant component in its direction would typically be broken for very small bead displacement, by being stretched beyond the tensile strength. Moreover, best-studied actin CLs like filamin or alpha-actinin typically unbind at even lower rupture forces of $40 - 80$ pN [4] and such unbinding and rebinding is thought to play a crucial role in viscoelastic response of cytoskeletal networks. At present, our modelling framework is stationary and does not account for dynamic CLs. We thus acknowledge that the model as it stands is not yet suitable for realistic description of crosslinked actin networks and postpone such considerations for future work.

S4 Upscaling and continuum model

S4.1 Details of discrete-to-continuum upscaling

S4.1.1 Upscaling the force balance

Denoting partial derivatives with subscripts, we can express the relevant finite differences using Taylor expansions as

$$\begin{aligned} &x_{i+1,j} - x_{i,j} = x(X_{i+1}, Y_j) - x(X_i, Y_j) = (X_{i+1} - X_i)x_X(X_i, Y_j) + \\ &\frac{(X_{i+1} - X_i)^2}{2} x_{XX}(X_i, Y_j) + O((X_{i+1} - X_i)^3) = \varepsilon x_X(X_i, Y_j) + \frac{\varepsilon^2}{2} x_{XX}(X_i, Y_j) + O(\varepsilon^3). \end{aligned} \tag{S17}$$

For other differences involving the deformed coordinate x occuring in our equations, we get

$$\begin{aligned} x_{i-1,j} - x_{i,j} &= -\varepsilon x_X(X_i, Y_j) + \frac{\varepsilon^2}{2} x_{XX}(X_i, Y_j) + O(\varepsilon^3) \\ x_{i,j+1} - x_{i,j} &= \varepsilon x_Y(X_i, Y_j) + \frac{\varepsilon^2}{2} x_{YY}(X_i, Y_j) + O(\varepsilon^3) \\ x_{i,j-1} - x_{i,j} &= -\varepsilon x_Y(X_i, Y_j) + \frac{\varepsilon^2}{2} x_{YY}(X_i, Y_j) + O(\varepsilon^3), \end{aligned} \tag{S18}$$

and analogous equations hold for y. For convenience, we omit the point at which the derivatives are evaluated from now on. In what follows we assume that all relevant partial derivatives of x and y are $O(1)$. Assuming $\varepsilon \ll 1$, we apply (S17)-(S18) to the dimensionless force balance (4) and bringing back the $1/(\varepsilon_c N) = \varepsilon/\varepsilon_c$ factor, we get

$$\begin{aligned} &\Bigg\{ \mathcal{F}\left(\xi\sqrt{\left(-x_X + \frac{\varepsilon}{2}x_{XX} + O(\varepsilon^2)\right)^2 + \left(-y_X + \frac{\varepsilon}{2}y_{XX} + O(\varepsilon^2)\right)^2}\right) \frac{\left(-x_X + \frac{\varepsilon}{2}x_{XX} + O(\varepsilon^2), -y_X + \frac{\varepsilon}{2}y_{XX} + O(\varepsilon^2)\right)}{\sqrt{\left(-x_X + \frac{\varepsilon}{2}x_{XX} + O(\varepsilon^2)\right)^2 + \left(-y_X + \frac{\varepsilon}{2}y_{XX} + O(\varepsilon^2)\right)^2}} + \\ &\mathcal{F}\left(\xi\sqrt{\left(x_X + \frac{\varepsilon}{2}x_{XX} + O(\varepsilon^2)\right)^2 + \left(y_X + \frac{\varepsilon}{2}y_{XX} + O(\varepsilon^2)\right)^2}\right) \frac{\left(x_X + \frac{\varepsilon}{2}x_{XX} + O(\varepsilon^2), y_X + \frac{\varepsilon}{2}y_{XX} + O(\varepsilon^2)\right)}{\sqrt{\left(x_X + \frac{\varepsilon}{2}x_{XX} + O(\varepsilon^2)\right)^2 + \left(y_X + \frac{\varepsilon}{2}y_{XX} + O(\varepsilon^2)\right)^2}} + \\ &\mathcal{F}\left(\xi\sqrt{\left(-x_Y + \frac{\varepsilon}{2}x_{YY} + O(\varepsilon^2)\right)^2 + \left(-y_Y + \frac{\varepsilon}{2}y_{YY} + O(\varepsilon^2)\right)^2}\right) \frac{\left(-x_Y + \frac{\varepsilon}{2}x_{YY} + O(\varepsilon^2), -y_Y + \frac{\varepsilon}{2}y_{YY} + O(\varepsilon^2)\right)}{\sqrt{\left(-x_Y + \frac{\varepsilon}{2}x_{YY} + O(\varepsilon^2)\right)^2 + \left(-y_Y + \frac{\varepsilon}{2}y_{YY} + O(\varepsilon^2)\right)^2}} + \\ &\mathcal{F}\left(\xi\sqrt{\left(x_Y + \frac{\varepsilon}{2}x_{YY} + O(\varepsilon^2)\right)^2 + \left(y_Y + \frac{\varepsilon}{2}y_{YY} + O(\varepsilon^2)\right)^2}\right) \frac{\left(x_Y + \frac{\varepsilon}{2}x_{YY} + O(\varepsilon^2), y_Y + \frac{\varepsilon}{2}y_{YY} + O(\varepsilon^2)\right)}{\sqrt{\left(x_Y + \frac{\varepsilon}{2}x_{YY} + O(\varepsilon^2)\right)^2 + \left(y_Y + \frac{\varepsilon}{2}y_{YY} + O(\varepsilon^2)\right)^2}} \Bigg\} \frac{\varepsilon}{\varepsilon_c} = \mathbf{0}. \end{aligned} \tag{S19}$$

Assuming $\varepsilon \ll 1$, we Taylor expand the denominators according to

$$\frac{1}{\sqrt{A + B\varepsilon + C\varepsilon^2 + O(\varepsilon^3)}} = \frac{1}{\sqrt{A}} - \frac{B\varepsilon}{2A^{3/2}} + \varepsilon^2 \frac{3B^2 - 4AC}{8A^{5/2}} + O(\varepsilon^3) \tag{S20}$$

and those in the discrete bending terms (with ε^2 cancelling out as a common term in both the numerator and denominator) according to

$$\frac{1}{A + B\varepsilon + O(\varepsilon^2)} = \frac{1}{A} - \frac{B\varepsilon}{A^2} + O(\varepsilon^2). \tag{S21}$$

The nonlinear force terms are expanded as

$$\mathcal{F}(\psi(\varepsilon)) = \mathcal{F}(\psi(0)) + \varepsilon \mathcal{F}'(\psi(0))\psi'(0) + O(\varepsilon^2) \tag{S22}$$

which holds for sufficiently smooth functions $\mathcal{F}$ and ψ. We denote

$$\lambda^X(X, Y) = \xi\sqrt{x_X^2 + y_X^2} \qquad \lambda^Y(X, Y) = \xi\sqrt{x_Y^2 + y_Y^2}$$

using which the $X-$component of the force balance can be simplified to

$$\left\{\left(-x_X+\frac{\varepsilon}{2}x_{XX}+O(\varepsilon^2)\right)\left(\frac{1}{\sqrt{x_X^2+y_X^2}}+\frac{\varepsilon(x_Xx_{XX}+y_Xy_{XX})}{2(x_X^2+y_X^2)^{3/2}}+O(\varepsilon^2)\right)\left(\mathcal{F}\left(\lambda^X\right)-\varepsilon\xi\mathcal{F}'\left(\lambda^X\right)\frac{x_Xx_{XX}+y_Xy_{XX}}{2\sqrt{x_X^2+y_X^2}}+O(\varepsilon^2)\right)+\right.$$
$$\left(x_X+\frac{\varepsilon}{2}x_{XX}+O(\varepsilon^2)\right)\left(\frac{1}{\sqrt{x_X^2+y_X^2}}-\frac{\varepsilon(x_Xx_{XX}+y_Xy_{XX})}{2(x_X^2+y_X^2)^{3/2}}+O(\varepsilon^2)\right)\left(\mathcal{F}\left(\lambda^X\right)+\varepsilon\xi\mathcal{F}'\left(\lambda^X\right)\frac{x_Xx_{XX}+y_Xy_{XX}}{2\sqrt{x_X^2+y_X^2}}+O(\varepsilon^2)\right)+$$
$$\left(-x_Y+\frac{\varepsilon}{2}x_{YY}+O(\varepsilon^2)\right)\left(\frac{1}{\sqrt{x_Y^2+y_Y^2}}+\frac{\varepsilon(x_Yx_{YY}+y_Yy_{YY})}{2(x_Y^2+y_Y^2)^{3/2}}+O(\varepsilon^2)\right)\left(\mathcal{F}\left(\lambda^Y\right)-\varepsilon\xi\mathcal{F}'\left(\lambda^Y\right)\frac{x_Yx_{YY}+y_Yy_{YY}}{2\sqrt{x_Y^2+y_Y^2}}+O(\varepsilon^2)\right)+$$
$$\left.\left(x_Y+\frac{\varepsilon}{2}x_{YY}+O(\varepsilon^2)\right)\left(\frac{1}{\sqrt{x_Y^2+y_Y^2}}-\frac{\varepsilon(x_Yx_{YY}+y_Yy_{YY})}{2(x_Y^2+y_Y^2)^{3/2}}+O(\varepsilon^2)\right)\left(\mathcal{F}\left(\lambda^Y\right)+\varepsilon\xi\mathcal{F}'\left(\lambda^Y\right)\frac{x_Yx_{YY}+y_Yy_{YY}}{2\sqrt{x_Y^2+y_Y^2}}+O(\varepsilon^2)\right)\right\}\frac{\varepsilon}{\varepsilon_c}=0 \tag{S23}$$

and the $Y-$component to

$$\left\{\left(-y_X+\frac{\varepsilon}{2}y_{XX}+O(\varepsilon^2)\right)\left(\frac{1}{\sqrt{x_X^2+y_X^2}}+\frac{\varepsilon(x_Xx_{XX}+y_Xy_{XX})}{2(x_X^2+y_X^2)^{3/2}}+O(\varepsilon^2)\right)\left(\mathcal{F}\left(\lambda^X\right)-\varepsilon\xi\mathcal{F}'\left(\lambda^X\right)\frac{x_Xx_{XX}+y_Xy_{XX}}{2\sqrt{x_X^2+y_X^2}}+O(\varepsilon^2)\right)+\right.$$
$$\left(y_X+\frac{\varepsilon}{2}y_{XX}+O(\varepsilon^2)\right)\left(\frac{1}{\sqrt{x_X^2+y_X^2}}-\frac{\varepsilon(x_Xx_{XX}+y_Xy_{XX})}{2(x_X^2+y_X^2)^{3/2}}+O(\varepsilon^2)\right)\left(\mathcal{F}\left(\lambda^X\right)+\varepsilon\xi\mathcal{F}'\left(\lambda^X\right)\frac{x_Xx_{XX}+y_Xy_{XX}}{2\sqrt{x_X^2+y_X^2}}+O(\varepsilon^2)\right)+$$
$$\left(-y_Y+\frac{\varepsilon}{2}y_{YY}+O(\varepsilon^2)\right)\left(\frac{1}{\sqrt{x_Y^2+y_Y^2}}+\frac{\varepsilon(x_Yx_{YY}+y_Yy_{YY})}{2(x_Y^2+y_Y^2)^{3/2}}+O(\varepsilon^2)\right)\left(\mathcal{F}\left(\lambda^Y\right)-\varepsilon\xi\mathcal{F}'\left(\lambda^Y\right)\frac{x_Yx_{YY}+y_Yy_{YY}}{2\sqrt{x_Y^2+y_Y^2}}+O(\varepsilon^2)\right)+$$
$$\left.\left(y_Y+\frac{\varepsilon}{2}y_{YY}+O(\varepsilon^2)\right)\left(\frac{1}{\sqrt{x_Y^2+y_Y^2}}-\frac{\varepsilon(x_Yx_{YY}+y_Yy_{YY})}{2(x_Y^2+y_Y^2)^{3/2}}+O(\varepsilon^2)\right)\left(\mathcal{F}\left(\lambda^Y\right)+\varepsilon\xi\mathcal{F}'\left(\lambda^Y\right)\frac{x_Yx_{YY}+y_Yy_{YY}}{2\sqrt{x_Y^2+y_Y^2}}+O(\varepsilon^2)\right)\right\}\frac{\varepsilon}{\varepsilon_c}=0. \tag{S24}$$

At $O(1)$ and $O(\varepsilon)$, the balance is automatically satisfied. Returning to vector form, at $O(\varepsilon^2)$ we get

$$\mathbf{0}=\frac{1}{\varepsilon_c}\left\{\mathcal{F}(\lambda^X)\left(\frac{(x_X,y_X)}{\sqrt{x_X^2+y_X^2}}\right)_X+\xi\frac{x_Xx_{XX}+y_Xy_{XX}}{x_X^2+y_X^2}\mathcal{F}'(\lambda^X)(x_X,y_X)+\mathcal{F}(\lambda^Y)\left(\frac{(x_Y,y_Y)}{\sqrt{x_Y^2+y_Y^2}}\right)_Y+\right.$$
$$\left.\xi\frac{x_Yx_{YY}+y_Yy_{YY}}{x_Y^2+y_Y^2}\mathcal{F}'(\lambda^Y)(x_Y,y_Y)\right\}.$$

Recalling the definitions of λ^X and λ^Y and multiplying by ε_c, we conclude the macroscale force balance (10).

S4.1.2 Deriving strain energy density

We further deduce the strain energy function for the derived continuum problem. As before, we nondimensionalize the lengths with respect to $\tilde{D}$ and the forces with $\pi\tilde{Y}\tilde{b}_c^2$ (so that the energies are nondimensionalized with $\pi\tilde{D}\tilde{Y}\tilde{b}_c^2$), Taylor expand the dimensional energy stored at CL (i,j) (S6) and upon further simplifications get

$$e_{i,j}(\varepsilon)=\frac{\varepsilon^2}{\varepsilon_c^2}\left(\mathcal{E}\left(\xi\sqrt{x_X^2+y_X^2}\right)+\mathcal{E}\left(\xi\sqrt{x_Y^2+y_Y^2}\right)+O(\varepsilon)\right),$$

where $\mathcal{E}$ is the dimensionless counterpart of the dimensional $\tilde{\mathcal{E}}$ defined in (S7). To arrive at macroscale strain energy density W, we divide by an area corresponding to one CL in the undeformed configuration ε^2 and sending $\varepsilon\to 0$ $(N\to\infty)$ obtain

$$W=\frac{1}{\varepsilon_c^2}\left(\mathcal{E}\left(\xi\sqrt{x_X^2+y_X^2}\right)+\mathcal{E}\left(\xi\sqrt{x_Y^2+y_Y^2}\right)\right). \tag{S25}$$

S4.2 Deducing the continuum problem under the linearized constitutive law

Under the linearized microscale constitutive law for vimentin (9), the continuum problem (10) takes (upon dividing by ξ) the form

$$\left((x_X,y_X)\max\left\{0,1-\frac{1}{\xi\sqrt{x_X^2+y_X^2}}\right\}\right)_X+\left((x_Y,y_Y)\max\left\{0,1-\frac{1}{\xi\sqrt{y_Y^2+x_Y^2}}\right\}\right)_Y=\mathbf{0}. \tag{S26}$$

We further state the dimensional stress tensor (11) under (9) to be

$$\tilde{\boldsymbol{S}} = \frac{\pi\tilde{Y}\tilde{b}_c^2}{\tilde{\Lambda}_c}\begin{pmatrix} \tilde{x}_{\tilde{X}} \max\left\{0, 1-\dfrac{1}{\xi\sqrt{\tilde{x}_{\tilde{X}}^2+\tilde{y}_{\tilde{X}}^2}}\right\} & \tilde{y}_{\tilde{X}} \max\left\{0, 1-\dfrac{1}{\xi\sqrt{\tilde{x}_{\tilde{X}}^2+\tilde{y}_{\tilde{X}}^2}}\right\} \\ \tilde{x}_{\tilde{Y}} \max\left\{0, 1-\dfrac{1}{\xi\sqrt{\tilde{x}_{\tilde{Y}}^2+\tilde{y}_{\tilde{Y}}^2}}\right\} & \tilde{y}_{\tilde{Y}} \max\left\{0, 1-\dfrac{1}{\xi\sqrt{\tilde{x}_{\tilde{Y}}^2+\tilde{y}_{\tilde{Y}}^2}}\right\} \end{pmatrix}, \tag{S27}$$

and the dimensional counterpart of (S26) then reads

$$\frac{\pi\tilde{Y}\tilde{b}_c^2}{\tilde{\Lambda}_c}\left\{\left((\tilde{x}_{\tilde{X}}, \tilde{y}_{\tilde{X}}) \max\left\{0, 1-\frac{1}{\xi\sqrt{\tilde{x}_{\tilde{X}}^2+\tilde{y}_{\tilde{X}}^2}}\right\}\right)_{\tilde{X}} + \left((\tilde{x}_{\tilde{Y}}, \tilde{y}_{\tilde{Y}}) \max\left\{0, 1-\frac{1}{\xi\sqrt{\tilde{y}_{\tilde{Y}}^2+\tilde{x}_{\tilde{Y}}^2}}\right\}\right)_{\tilde{Y}}\right\} = \boldsymbol{0}, \tag{S28}$$

which is used in continuum simulations. Using the displacement field

$$\tilde{u}(\tilde{X}, \tilde{Y}) = \tilde{x}(\tilde{X}, \tilde{Y}) - \tilde{X} \qquad \tilde{v}(\tilde{X}, \tilde{Y}) = \tilde{y}(\tilde{X}, \tilde{Y}) - \tilde{Y},$$

this can be rewritten as

$$\frac{\pi\tilde{Y}\tilde{b}_c^2}{\tilde{\Lambda}_c}\left\{\left((1+\tilde{u}_{\tilde{X}}, \tilde{v}_{\tilde{X}}) \max\left\{0, 1-\frac{1}{\xi\sqrt{(1+\tilde{u}_{\tilde{X}})^2+\tilde{v}_{\tilde{X}}^2}}\right\}\right)_{\tilde{X}} + \left((\tilde{u}_{\tilde{Y}}, 1+\tilde{v}_{\tilde{Y}}) \max\left\{0, 1-\frac{1}{\xi\sqrt{\tilde{u}_{\tilde{Y}}^2+(1+\tilde{v}_{\tilde{Y}})^2}}\right\}\right)_{\tilde{Y}}\right\} = \boldsymbol{0}. \tag{S29}$$

S4.3 Strain energy density and nominal stress tensor

S4.3.1 Relation to nonlinear elasticity models for fiber-reinforced materials

Redimensionalizing (S25) (in order to facilitate comparison with the standard results on fiber-reinforced materials), the strain energy density can be rewritten in terms of the deformation gradient tensor $\boldsymbol{F}$ with components $F_{kl} = \partial\tilde{x}_i/\partial\tilde{X}_j$ or in terms of the right Cauchy-Green deformation tensor $\boldsymbol{C} = \boldsymbol{F}^T\boldsymbol{F}$ as

$$\tilde{W} = \frac{\tilde{\mathcal{E}}\left(\xi\sqrt{F_{11}^2+F_{21}^2}\right) + \tilde{\mathcal{E}}\left(\xi\sqrt{F_{12}^2+F_{22}^2}\right)}{\tilde{R}_c^2} = \frac{\tilde{\mathcal{E}}\left(\xi\sqrt{C_{11}}\right) + \tilde{\mathcal{E}}\left(\xi\sqrt{C_{22}}\right)}{\tilde{R}_c^2}. \tag{S30}$$

Introducing $\boldsymbol{M} = (1, 0)$ and $\boldsymbol{M'} = (0, 1)$ as the two directions of filaments in the undeformed configuration and employing the theory of fiber-reinforced materials, two invariants corresponding to these directions take forms $I_4 = \boldsymbol{M}\cdot(\boldsymbol{C}\boldsymbol{M}) = C_{11}$ and $I_6 = \boldsymbol{M'}\cdot(\boldsymbol{C}\boldsymbol{M'}) = C_{22}$. We can therefore express $\tilde{W}$ also in terms of the invariants of $\boldsymbol{C}$ as (12), thus establishing connection to the rich literature on constitutive modelling of fiber-reinforced materials. Using (S8), we can express this strain energy density as

$$\tilde{W}(\boldsymbol{C}) = \frac{2\displaystyle\int_{\xi_{sf}}^{\xi}\tilde{\mathcal{F}}(t)dt + \int_{\xi}^{\xi\sqrt{I_4(\boldsymbol{C})}}\tilde{\mathcal{F}}(t)dt + \int_{\xi}^{\xi\sqrt{I_6(\boldsymbol{C})}}\tilde{\mathcal{F}}(t)dt}{\xi\tilde{R}_c}, \tag{S31}$$

where ξ_{sf} denotes the normalized stress-free end-to-end distance so that the first integral represents the strain energy stored in the undeformed domain due to pre-stress (noting that in the undeformed configuration one has $\boldsymbol{F} = \boldsymbol{I}$ and $I_4(\boldsymbol{C}) = I_6(\boldsymbol{C}) = 1$) and the last two integrals represent the elastically-stored energy supplied with the deformation. Finally, assuming the approximation (9), the strain energy density (12) can be written as

$$\tilde{W}(\boldsymbol{C}) = \frac{\pi\tilde{Y}\tilde{b}_c^2\xi}{2\tilde{R}_c}\left[\max\left(0, \sqrt{I_4(\boldsymbol{C})} - \frac{1}{\xi}\right)^2 + \max\left(0, \sqrt{I_6(\boldsymbol{C})} - \frac{1}{\xi}\right)^2\right], \tag{S32}$$

where ξ is approximated using (8). The problem (S29) can thus be re-formulated in the framework of nonlinear elasticity as minimization of the strain energy (S32). We further propose a smooth approximation to the microscale constitutive law and using

$$\max(0, x) \approx \frac{x}{1+e^{-\kappa x}}, \tag{S33}$$

which provides a good approximation to the maximum function for large κ, we get a smooth approximation to the strain energy

$$\tilde{W}(\boldsymbol{C}) = \frac{\pi\tilde{Y}\tilde{b}_c^2\xi}{2\tilde{R}_c}\left[\left(\frac{\sqrt{I_4(\boldsymbol{C})}-1/\xi}{1+e^{-\kappa\left(\sqrt{I_4(\boldsymbol{C})}-1/\xi\right)}}\right)^2+\left(\frac{\sqrt{I_6(\boldsymbol{C})}-1/\xi}{1+e^{-\kappa\left(\sqrt{I_6(\boldsymbol{C})}-1/\xi\right)}}\right)^2\right], \tag{S34}$$

the minimization of which is implemented in our FEniCS code. Figure S6 documents that the approximation (S33) with $\kappa = 200$ leads to only negligible changes in the microscale constitutive law for vimentin.

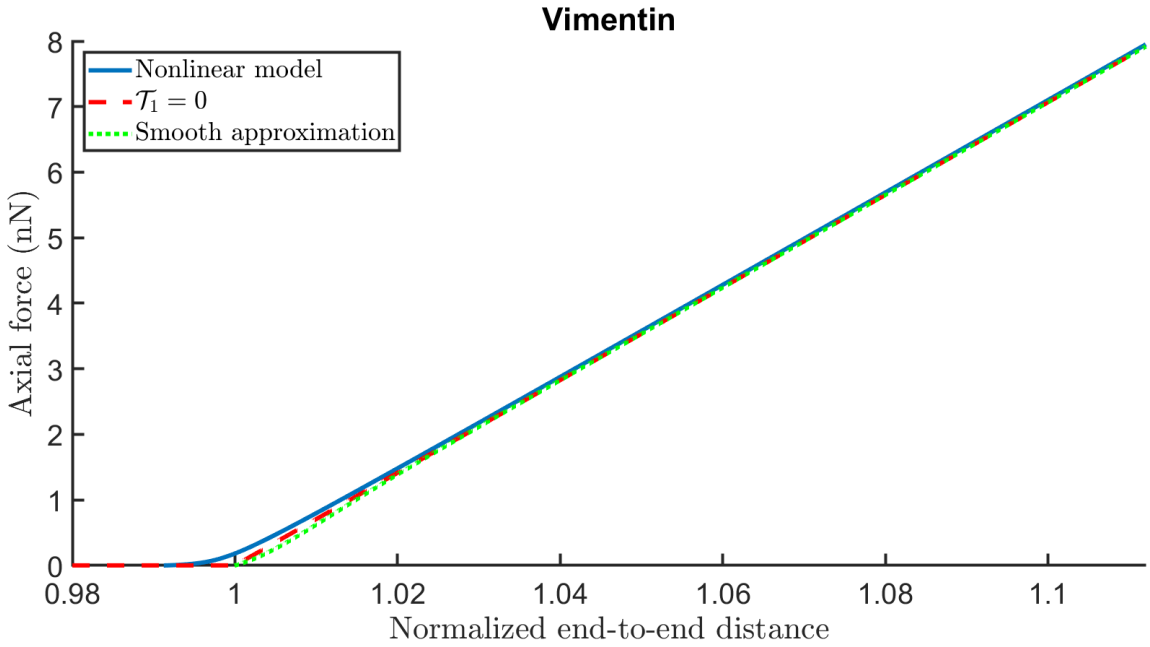

Figure S6: The smooth approximation (S33) with $\kappa = 200$ yields negligible changes to the microscale constitutive law for vimentin.

S4.3.2 Stress tensor

Next, we deduce the components of the nominal stress tensor $\tilde{\boldsymbol{S}}$ from $\tilde{S}_{kl} = \partial\tilde{W}/\partial F_{ji}$ getting (11). Storm et al. [11] applied the Doi-Edwards construction [3] to a crosslinked network with an arbitrary distribution $\tilde{\Psi}$ of end-to-end separation vectors $\tilde{\boldsymbol{r}}$ and arrived at an averaged Cauchy stress tensor $\tilde{\boldsymbol{\sigma}}$ of the form

$$\tilde{\sigma}_{kl}^T = \frac{\tilde{\varrho}}{\det(\boldsymbol{F})}\left\langle \tilde{f}(|\boldsymbol{F}\tilde{\boldsymbol{r}}|)\frac{F_{il}\tilde{r}_l F_{jk}\tilde{r}_k}{|\boldsymbol{F}\tilde{\boldsymbol{r}}|}\right\rangle_{\tilde{\Psi}(\tilde{\boldsymbol{r}})}$$

where $\tilde{\varrho}$ denotes the number of FSs per unit volume (otherwise their notation coincides with ours). Note that the microscale force was given as function of the dimensional end-to-end distance $\tilde{r}$, as opposed to the dimensionless distance r. Letting $\tilde{\delta}(\tilde{\boldsymbol{r}})$ denote the Dirac delta function centered at $\tilde{\boldsymbol{r}} = \boldsymbol{0}$ and applying this formula to our two-dimensional case with

$$\tilde{\Psi}(\tilde{\boldsymbol{r}}) = \frac{1}{4}\left\{\tilde{\delta}(\tilde{\boldsymbol{r}}-(\tilde{R},0))+\tilde{\delta}(\tilde{\boldsymbol{r}}-(-\tilde{R},0))+\tilde{\delta}(\tilde{\boldsymbol{r}}-(0,\tilde{R}))+\tilde{\delta}(\tilde{\boldsymbol{r}}-(0,-\tilde{R}))\right\}$$

reflecting the undeformed orientations of filaments in our geometry and with $\tilde{\varrho} = 2N^2/\tilde{D}^2$, we arrive at a result identical to the one obtained when the connection $\tilde{\boldsymbol{\sigma}}^T = \det(\boldsymbol{F})^{-1}\tilde{\boldsymbol{S}}^T\boldsymbol{F}^T$ from nonlinear elasticity [9] is applied to (11), which further certifies the correctness of our results.

S5 Details of the small-deformations and small-bead analysis

S5.1 Deriving small-deformations limit

Substituting (17) into (10) we get

$$\mathbf{0} = \left(\mathcal{F}\left(\xi \sqrt{(1+R_b\hat{x}_X)^2 + (R_b\hat{y}_X)^2 + O(R_b^2)} \right) \frac{(1+R_b\hat{x}_X + O(R_b^2), R_b\hat{y}_X + O(R_b^2))}{\sqrt{(1+R_b\hat{x}_X)^2 + (R_b\hat{y}_X)^2 + O(R_b^2)}} \right)_X + \left(\mathcal{F}\left(\xi \sqrt{(R_b\hat{x}_Y)^2 + (1+R_b\hat{y}_Y)^2 + O(R_b^2)} \right) \frac{(R_b\hat{x}_Y + O(R_b^2), 1+R_b\hat{y}_Y + O(R_b^2))}{\sqrt{(R_b\hat{x}_Y)^2 + (1+R_b\hat{y}_Y)^2 + O(R_b^2)}} \right)_Y . \tag{S35}$$

Taylor expanding $\mathcal{F}$ as well as the denominators for $R_b \ll 1$, we get

$$\mathbf{0} = \left(\left(\mathcal{F}(\xi) + R_b\xi\mathcal{F}'(\xi)\hat{x}_X + O(R_b^2) \right) (1 + R_b\hat{x}_X + O(R_b^2), R_b\hat{y}_X + O(R_b^2)) \left(1 - R_b\hat{x}_X + O(R_b^2) \right) \right)_X + \left(\left(\mathcal{F}(\xi) + R_b\xi\mathcal{F}'(\xi)\hat{y}_Y + O(R_b^2) \right) (R_b\hat{x}_Y + O(R_b^2), 1 + R_b\hat{y}_Y + O(R_b^2)) \left(1 - R_b\hat{y}_Y + O(R_b^2) \right) \right)_Y . \tag{S36}$$

The balance at $O(1)$ is trivially satisfied. At $O(R_b)$, we get (18)-(19) in the main text.

S5.2 Details of small-bead asymptotics

S5.2.1 $\hat{x}$ problem

We split the analysis into the inner (boundary) region characterized by

$$\frac{X}{a} = \bar{X} = O(1) \quad \frac{Y}{a} = \bar{Y} = O(1)$$

where we use the ansatz for inner solution

$$\hat{x}^I(\bar{X}, \bar{Y}, a) = \hat{x}_0^I(\bar{X}, \bar{Y}) + \frac{1}{\ln(1/a)}\hat{x}_1^I(\bar{X}, \bar{Y}) + \frac{1}{\ln^2(1/a)}\hat{x}_2^I(\bar{X}, \bar{Y}) + O\left(\frac{1}{\ln^3(1/a)}\right)$$

satisfying the boundary condition at $\bar{X}^2 + \bar{Y}^2 = 1$, and the outer region $X = O(1) = Y$ with the outer solution

$$\hat{x}^O(X, Y, a) = \hat{x}_0^O(X, Y) + \frac{1}{\ln(1/a)}\hat{x}_1^O(X, Y) + \frac{1}{\ln^2(1/a)}\hat{x}_2^O(\bar{X}, \bar{Y}) + O\left(\frac{1}{\ln^3(1/a)}\right)$$

satisfying the Dirichlet condition at the outer boundary $\hat{x}^O = 0$. The rationale behind the logarithmic terms in the expansions will become apparent in the course of the analysis. In the inner region, we transform the $\bar{Y}$ coordinate according to $\bar{Y} = \sqrt{\omega}\bar{Z}$ so that we get Laplace's equation for the leading-order inner solution

$$\hat{x}^I_{0,\bar{X}\bar{X}} + \hat{x}^I_{0,\bar{Z}\bar{Z}} = 0$$

on a domain with an ellipse cut out of it as depicted in Figure 5. We introduce elliptical coordinates

$$\bar{X} = c\sinh(\mu)\sin(\nu) \qquad \bar{Z} = c\cosh(\mu)\cos(\nu) \tag{S37}$$

where $c = \sqrt{(1-\omega)/\omega}$ is the (linear) eccentricity of the inner ellipse, $(\mu, \nu) \in (\mu_1, \infty) \times [0, 2\pi]$ so that $\mu = \mu_1 = \cosh^{-1}\left((1-\omega)^{-1/2}\right)$ represents the elliptical (inner) boundary. Note that even if our outer domain boundary is a circle in (X, Y) coordinates (a square domain being even less amenable to analysis), in $(\bar{X}, \bar{Z})$ coordinates it transforms into an ellipse with the same eccentricity as the inner (bead) elliptic boundary and therefore it cannot be simply characterized by $\mu = \mu_2$ for some $\mu_2 > \mu_1$ (because the eccentricity of ellipses given by $\mu =$ constant in elliptical coordinates strictly decreases with μ). This causes the full problem (with $a > 0$) to be analytically intractable and forced us to only study the $a \ll 1$ limit. Writing $\Phi_0^I(\mu, \nu) = \hat{x}_0^I(\bar{X}, \bar{Z})$ we then have $\Phi_0^I(\mu_1, \nu) = \cos(\varphi_*)$ for all ν and

$$\frac{1}{c^2(\cosh^2(\mu) + \sin^2(\nu))}\left(\Phi^I_{0,\mu\mu} + \Phi^I_{0,\nu\nu}\right) = 0$$

and thus

$$\Phi^I_{0,\mu\mu} + \Phi^I_{0,\nu\nu} = 0.$$

We assume Φ_0^I to be $2\pi-$periodic in ν. As nothing drives the variation in ν in the inner layer, we search for a solution in the form $\Phi_0^I(\mu, \nu) = \Phi_0^I(\mu)$ solving $\Phi^I_{0,\mu\mu} = 0$. The solution reads $\Phi_0^I = A_0\mu + B_0$. Following the same

line of reasoning, we get that the higher-order terms $\Phi_i^I(\mu,\nu) = \hat{x}_i^I(\bar{X},\bar{Z})$ are of the same form $\Phi_i^I = A_i\mu + B_i$. We transform back to Cartesian coordinates [12] so that

$$\mu = \frac{1}{2}\ln\left(1 - 2q(\bar{X},\bar{Z}) + 2\sqrt{q^2(\bar{X},\bar{Z}) - q(\bar{X},\bar{Z})}\right) \tag{S38}$$

with

$$q(\bar{X},\bar{Z}) = \frac{-(\bar{X}^2+\bar{Z}^2-c^2) - \sqrt{(\bar{X}^2+\bar{Z}^2-c^2)^2 + 4c^2\bar{X}^2}}{2c^2}.$$

In $(\bar{X},\bar{Y})$ variables and expressed using ω, q reads (25). Next we wish to write $\hat{x}_0^I$ in the outer coordinates (X,Z) for the purposes of matching with the outer layer. To do this, we first rewrite q in these variables and expand in a as

$$q = \frac{-(X/a)^2 - (Z/a)^2 + c^2 - \sqrt{\left((X/a)^2 + (Z/a)^2 - c^2\right)^2 + 4c^2(X/a)^2}}{2c^2} =$$

$$\frac{-(X/a)^2 - (Z/a)^2 + c^2 - 1/a^2 \times \sqrt{(X^2+Z^2)^2 + a^2c^2(2X^2-2Z^2) + a^4c^4}}{2c^2} = \frac{1}{a^2}\left(-\frac{X^2+Z^2}{c^2}\right) + O(1)$$

and then substitute it into (S38) to get

$$\mu = \frac{1}{2}\ln\left(1 + \frac{2(X^2+Z^2)}{a^2c^2} + O(1) + 2\sqrt{\left(\frac{X^2+Z^2}{a^2c^2}\right)^2 + O\left(\frac{1}{a^2}\right) + \frac{X^2+Z^2}{a^2c^2} + O(1)}\right) =$$

$$\frac{1}{2}\ln\left(\frac{4(X^2+Z^2)}{a^2c^2} + O(1)\right) = \ln\left(\frac{1}{a}\right) + \ln\left(\frac{2}{c}\sqrt{X^2+Z^2}\right) + O(a^2).$$

Thus we see that A_0 must equal 0 because otherwise the matching would require a contribution of order $\ln(1/a) \gg 1$ to exist in the outer solution. The inner boundary condition at the leading order then enforces $B_0 = \cos(\varphi_*)$. Our inner approximation thus so far reads

$$\hat{x}^I = \cos(\varphi_*) + \frac{1}{\ln(1/a)}(A_1\mu + B_1) + \frac{1}{\ln^2(1/a)}(A_2\mu + B_2) + O\left(\frac{1}{\ln^3(1/a)}\right) \tag{S39}$$

and writing this in outer variables we get

$$\cos(\varphi_*) + A_1 + O\left(\frac{1}{\ln(1/a)}\right). \tag{S40}$$

The leading order outer solution satisfies Laplace's equation (in (X,Z) variables) and Dirichlet boundary condition $\hat{x}_0^O = 0$ at the outer boundary. Irrespective of whether we assume this outer boundary to be a circle or a square in the original - i.e. (X,Y) - variables, the only admissible constant solution to this problem is $\hat{x}_0^O \equiv 0$. Comparing this with (S40) we conclude that the matching requires $A_1 = -\cos(\varphi_*)$. Finally, to satisfy the inner boundary condition at $O\left(\frac{1}{\ln(1/a)}\right)$, we must have $B_1 = -A_1\mu_1 = \cos(\varphi_*)\cosh^{-1}\left((1-\omega)^{-1/2}\right)$. Substituting A_1 and B_1 back into (S39) we get

$$\hat{x}^I = \cos(\varphi_*) + \frac{\cos(\varphi_*)\left(-\mu + \cosh^{-1}\left((1-\omega)^{-1/2}\right)\right)}{\ln(1/a)} + \frac{1}{\ln^2(1/a)}(A_2\mu + B_2) + O\left(\frac{1}{\ln^3(1/a)}\right). \tag{S41}$$

Writing this in outer variables we get

$$0 + \frac{1}{\ln(1/a)}\left(\cos(\varphi_*)\left(-\ln(2/c) - \ln\left(\sqrt{X^2+Z^2}\right) + \cosh^{-1}\left((1-\omega)^{-1/2}\right)\right) + A_2\right). \tag{S42}$$

Note that to match the $\ln\left(\sqrt{X^2+Z^2}\right)$ behaviour, the first-order correction in the outer solution must satisfy

$$\hat{x}^O_{1\,XX} + \hat{x}^O_{1\,ZZ} = -2\pi\cos(\varphi_*)\delta_{(0,0)},$$

where $\delta_{(0,0)}$ denotes the Dirac delta function (centered at the origin), and must vanish at the outer boundary. Matching further requires $A_2 = \cos(\varphi_*)\left(\ln(2/c) - \cosh^{-1}\left((1-\omega)^{-1/2}\right)\right)$. The inner boundary condition at this order implies $B_2 = -\cosh^{-1}\left((1-\omega)^{-1/2}\right)\cos(\varphi_*)\left(\ln(2/c) - \cosh^{-1}\left((1-\omega)^{-1/2}\right)\right)$. By induction, we can deduce the form of general A_i and B_i, getting $A_0 = 0$, $B_0 = \cos(\varphi_*)$ and for $i \geq 1$

$$A_i = -\cos(\varphi_*)\left(\cosh^{-1}\left((1-\omega)^{-1/2}\right) - \ln(2/c)\right)^{i-1} \qquad B_i = -\cosh^{-1}\left((1-\omega)^{-1/2}\right)A_i. \tag{S43}$$

The inner expansion thus reads

$$\hat{x}^I = \cos(\varphi_*) + \sum_{i=1}^{\infty} \frac{A_i\mu + B_i}{\ln^i(1/a)} + O(a)$$

which using (S43) and the formula for the sum of an infinite geometric series gives

$$\hat{x}^I = \cos(\varphi_*)\left(1 + \frac{\cosh^{-1}\left((1-\omega)^{-1/2}\right) - \mu}{\ln(1/a)} \sum_{i=1}^{\infty} \left(\frac{\cosh^{-1}\left((1-\omega)^{-1/2}\right) - \ln(2/c)}{\ln(1/a)}\right)^{i-1}\right) + O(a) =$$

$$= \cos(\varphi_*)\left(1 + \frac{\cosh^{-1}\left((1-\omega)^{-1/2}\right) - \mu}{\ln(1/a) + \ln(2/c) - \cosh^{-1}\left((1-\omega)^{-1/2}\right)}\right) + O(a).$$

Substituting μ from (S38) and expressing c in terms of ω, we arrive at (24).

S5.2.2 $\hat{y}$ problem

The equation for $\hat{y}$ becomes Laplace's equation after transforming the $\bar{X}$ coordinate according to $\bar{X} = \sqrt{\omega}\bar{W}$ (keeping $\bar{Y}$) and we have the boundary condition $\hat{y} = \sin(\varphi_*)$ at the inner ellipse. We then must transform to elliptical coordinates (ellipses now being oriented along the $\bar{W}$ axis rather than $\bar{Z}$ axis) as

$$\bar{Y} = c\sinh(\mu)\sin(\nu) \qquad \bar{W} = c\cosh(\mu)\cos(\nu) \tag{S44}$$

where again $c = \sqrt{(1-\omega)/\omega}$ is the (linear) eccentricity of the inner ellipse and $\mu_1 = \cosh^{-1}\left((1-\omega)^{-1/2}\right)$ denotes the (inner) elliptical boundary. The solutions to the resulting inner problems again read $C_i\mu + D_i$ and we again have

$$\mu = \frac{1}{2}\ln\left(1 - 2q_2(\bar{W},\bar{Y}) + 2\sqrt{q_2^2(\bar{W},\bar{Y}) - q_2(\bar{W},\bar{Y})}\right) \tag{S45}$$

where we now have

$$q_2(\bar{W},\bar{Y}) = \frac{-(\bar{W}^2 + \bar{Y}^2 - c^2) - \sqrt{(\bar{W}^2 + \bar{Y}^2 - c^2)^2 + 4c^2\bar{Y}^2}}{2c^2}.$$

In $(\bar{X},\bar{Y})$ variables and expressed using ω, q_2 reads (27). As before, we write the inner solutions in terms of the outer variable and conclude that in order to match we must have $C_0 = 0$ and inner boundary condition at the leading order gives $D_0 = \sin(\varphi_*)$. At the higher orders, we (analogous to the $\hat{x}$ case) conclude

$$C_i = -\sin(\varphi_*)\left(\cosh^{-1}\left((1-\omega)^{-1/2}\right) - \ln(2/c)\right)^{i-1} \qquad D_i = -\cosh^{-1}\left((1-\omega)^{-1/2}\right)C_i \tag{S46}$$

which leads to the inner expansion (26) for $\hat{y}$.

S5.3 Leading-order approximations to the strain fields for small beads

We get

$$\hat{x}^I_{X/Y} = -\frac{\cos(\varphi_*)}{2\ln(1/a) + \ln(4\omega/(1-\omega)) - 2\cosh^{-1}\left((1-\omega)^{-1/2}\right)} \frac{1}{1 - 2q + 2\sqrt{q^2-q}}\left(-2 + \frac{2q-1}{\sqrt{q^2-q}}\right)\frac{1}{a}\frac{\partial q}{\partial \bar{X}/\bar{Y}} + O(1) =$$

$$\frac{1}{a}\frac{\cos(\varphi_*)}{2\ln(1/a) + \ln(4\omega/(1-\omega)) - 2\cosh^{-1}\left((1-\omega)^{-1/2}\right)} \frac{1}{\sqrt{q^2-q}}\frac{\partial q}{\partial \bar{X}/\bar{Y}} + O(1) \tag{S47}$$

$$\hat{y}^I_{X/Y} = \frac{1}{a}\frac{\sin(\varphi_*)}{2\ln(1/a) + \ln(4\omega/(1-\omega)) - 2\cosh^{-1}\left((1-\omega)^{-1/2}\right)} \frac{1}{\sqrt{q_2^2-q_2}}\frac{\partial q_2}{\partial \bar{X}/\bar{Y}} + O(1) \tag{S48}$$

where $q(\bar{X},\bar{Y})$ and $q_2(\bar{X},\bar{Y})$ are given by (25) and (27). We have

$$\begin{aligned}
\frac{\partial q}{\partial \bar{X}} &= -\frac{\omega\bar{X}}{1-\omega}\left(1 + \frac{\omega\bar{X}^2 + \bar{Y}^2 + (1-\omega)}{\sqrt{(\omega\bar{X}^2 + \bar{Y}^2 - (1-\omega))^2 + 4(1-\omega)\omega\bar{X}^2}}\right),\\
\frac{\partial q}{\partial \bar{Y}} &= -\frac{\bar{Y}}{1-\omega}\left(1 + \frac{\omega\bar{X}^2 + \bar{Y}^2 - (1-\omega)}{\sqrt{(\omega\bar{X}^2 + \bar{Y}^2 - (1-\omega))^2 + 4(1-\omega)\omega\bar{X}^2}}\right),\\
\frac{\partial q_2}{\partial \bar{X}} &= -\frac{\bar{X}}{1-\omega}\left(1 + \frac{\bar{X}^2 + \omega\bar{Y}^2 - (1-\omega)}{\sqrt{(\bar{X}^2 + \omega\bar{Y}^2 - (1-\omega))^2 + 4(1-\omega)\omega\bar{Y}^2}}\right),\\
\frac{\partial q_2}{\partial \bar{Y}} &= -\frac{\omega\bar{Y}}{1-\omega}\left(1 + \frac{\bar{X}^2 + \omega\bar{Y}^2 + (1-\omega)}{\sqrt{(\bar{X}^2 + \omega\bar{Y}^2 - (1-\omega))^2 + 4(1-\omega)\omega\bar{Y}^2}}\right).
\end{aligned} \tag{S49}$$

S5.4 Calculating net force exerted on a small bead

Parameterizing the circle as $(\bar{X},\bar{Y})=(\cos(\varphi),\sin(\varphi))$, we get the unit normal vector $\boldsymbol{N}=(\cos(\varphi),\sin(\varphi))$ (pointing into the material) in the undeformed configuration and we calculate the total force exerted on the bead by the material as a line integral over the circle of dimensional radius $a\tilde{D}$ and thus

$$\tilde{\boldsymbol{F}}_b=\frac{\pi\tilde{Y}\tilde{b}_c^2}{\tilde{R}_c}\int_0^{2\pi}\begin{pmatrix}\mathcal{F}(\xi)+R_b\xi\mathcal{F}'(\xi)\hat{x}_X^I+O(R_b^2) & R_b\mathcal{F}(\xi)\hat{x}_Y^I+O(R_b^2)\\ R_b\mathcal{F}(\xi)\hat{y}_X^I+O(R_b^2) & \mathcal{F}(\xi)+R_b\xi\mathcal{F}'(\xi)\hat{y}_Y^I+O(R_b^2)\end{pmatrix}\begin{pmatrix}\cos(\varphi)\\ \sin(\varphi)\end{pmatrix}a\tilde{D}d\varphi=$$
$$\frac{\pi\tilde{Y}\tilde{b}_c^2aR_b\xi\mathcal{F}'(\xi)}{\varepsilon_c}\int_0^{2\pi}\begin{pmatrix}\hat{x}_X^I & \omega\hat{x}_Y^I\\ \omega\hat{y}_X^I & \hat{y}_Y^I\end{pmatrix}\begin{pmatrix}\cos(\varphi)\\ \sin(\varphi)\end{pmatrix}d\varphi+O(R_b^2). \tag{S50}$$

Notice that the leading-order contributions (i.e. $O(1)$ in R_b) cancel out. We calculate the leading-order approximation for the $X-$ and $Y-$components of the net force using (S47)-(S48) as

$$\begin{aligned}\tilde{F}_b^X=&\frac{\cos(\varphi_*)\pi\tilde{Y}\tilde{b}_c^2R_b\xi\mathcal{F}'(\xi)}{\varepsilon_c\left(2\ln(1/a)+\ln(4\omega/(1-\omega))-2\cosh^{-1}\left((1-\omega)^{-1/2}\right)\right)}\int_0^{2\pi}\frac{1}{\sqrt{q^2-q}}\left(\frac{\partial q}{\partial\bar{X}}\cos(\varphi)+\omega\frac{\partial q}{\partial\bar{Y}}\sin(\varphi)\right)d\varphi+O(a)\\ \tilde{F}_b^Y=&\frac{\sin(\varphi_*)\pi\tilde{Y}\tilde{b}_c^2R_b\xi\mathcal{F}'(\xi)}{\varepsilon_c\left(2\ln(1/a)+\ln(4\omega/(1-\omega))-2\cosh^{-1}\left((1-\omega)^{-1/2}\right)\right)}\int_0^{2\pi}\frac{1}{\sqrt{q_2^2-q_2}}\left(\omega\frac{\partial q_2}{\partial\bar{X}}\cos(\varphi)+\frac{\partial q_2}{\partial\bar{Y}}\sin(\varphi)\right)d\varphi+O(a)\end{aligned} \tag{S51}$$

S5.4.1 Evaluating the integrands at the bead

Evaluating (25) at the bead $(\bar{X},\bar{Y})=(\cos(\varphi),\sin(\varphi))$ and using $\sin^2(\varphi)=1-\cos^2(\varphi)$, we get

$$\begin{aligned}q(\varphi)=&\frac{-\omega\cos^2(\varphi)-\sin^2(\varphi)+(1-\omega)-\sqrt{(\omega\cos^2(\varphi)+\sin^2(\varphi)-(1-\omega))^2+4(1-\omega)\omega\cos^2(\varphi)}}{2(1-\omega)}\\ =&\frac{(1-\omega)\cos^2(\varphi)-\omega-\sqrt{(\omega-(1-\omega)\cos^2(\varphi))^2+4(1-\omega)\omega\cos^2(\varphi)}}{2(1-\omega)}=-\frac{\omega}{1-\omega}\end{aligned} \tag{S52}$$

and conclude

$$\frac{1}{\sqrt{q^2-q}}=\frac{1-\omega}{\sqrt{\omega}}.$$

Analogously, it is easy to show that $q_2=q$ at the bead and thus

$$\frac{1}{\sqrt{q_2^2-q_2}}=\frac{1-\omega}{\sqrt{\omega}}$$

Similarly, using (S49), the same trigonometric identity and our knowledge on what the square root term in (S52) simplifies into, we get at the bead

$$\frac{\partial q}{\partial\bar{X}}\cos(\varphi)+\omega\frac{\partial q}{\partial\bar{Y}}\sin(\varphi)=$$
$$-\frac{\omega}{1-\omega}\left\{\cos^2(\varphi)\left(1+\frac{\omega\cos^2(\varphi)+\sin^2(\varphi)+(1-\omega)}{\sqrt{(\omega\cos^2(\varphi)+\sin^2(\varphi)-(1-\omega))^2+4\omega(1-\omega)\cos^2(\varphi)}}\right)+\right.$$
$$\left.\sin^2(\varphi)\left(1+\frac{\omega\cos^2(\varphi)+\sin^2(\varphi)-(1-\omega)}{\sqrt{(\omega\cos^2(\varphi)+\sin^2(\varphi)-(1-\omega))^2+4\omega(1-\omega)\cos^2(\varphi)}}\right)\right\}=$$
$$-\frac{\omega}{1-\omega}\left\{1+\frac{\cos^2(\varphi)(2-\omega+(\omega-1)\cos^2(\varphi))+(1-\cos^2(\varphi))(\omega+(\omega-1)\cos^2(\varphi))}{\omega+(1-\omega)\cos^2(\varphi)}\right\}=-\frac{2\omega}{1-\omega}$$

and following the same steps also

$$\omega\frac{\partial q_2}{\partial\bar{X}}\cos(\varphi)+\frac{\partial q_2}{\partial\bar{Y}}\sin(\varphi)=-\frac{2\omega}{1-\omega}.$$

Substituting back into (S51) we get

$$\tilde{\boldsymbol{F}}_b = -(\cos(\varphi_*), \sin(\varphi_*))\tilde{F}_b^0 + O(a), \tag{S53}$$

where

$$\tilde{F}_b^0 = \frac{2\pi R_b/\varepsilon_c\sqrt{\xi\mathcal{F}(\xi)\mathcal{F}'(\xi)}}{\ln(1/a) + \ln(2\sqrt{\omega/(1-\omega)}) - \cosh^{-1}((1-\omega)^{-\frac{1}{2}})}\pi\tilde{Y}\tilde{b}_c^2. \tag{S54}$$

Using the constitutive law (9) and simplifying, the leading-order dimensionless net force can be written as

$$\begin{aligned} F_b^0 &= \frac{2\pi R_b/\varepsilon_c\sqrt{\mathcal{F}_p(1+\mathcal{F}_p)}}{\ln(2\sqrt{\mathcal{F}_p}/a) - \cosh^{-1}(\sqrt{1+\mathcal{F}_p})} = \frac{2\pi R_b/\varepsilon_c\sqrt{\mathcal{F}_p(1+\mathcal{F}_p)}}{\ln(2\sqrt{\mathcal{F}_p}/a) - \ln(\sqrt{1+\mathcal{F}_p} + \sqrt{\mathcal{F}_p})} \\ &\frac{2\pi R_b/\varepsilon_c\sqrt{\mathcal{F}_p(1+\mathcal{F}_p)}}{\ln\left(\dfrac{2\sqrt{\mathcal{F}_p}}{a\left(\sqrt{1+\mathcal{F}_p} + \sqrt{\mathcal{F}_p}\right)}\right)} = \frac{2\pi R_b/\varepsilon_c\sqrt{\mathcal{F}_p(1+\mathcal{F}_p)}}{\ln\left(\dfrac{2\left(\sqrt{\mathcal{F}_p(1+\mathcal{F}_p)} - \mathcal{F}_p\right)}{a}\right)}, \end{aligned} \tag{S55}$$

which gives (29)-(30).

References

[1] Johanna Block, Hannes Witt, Andrea Candelli, Erwin JG Peterman, Gijs JL Wuite, Andreas Janshoff, and Sarah Köster. Nonlinear loading-rate-dependent force response of individual vimentin intermediate filaments to applied strain. *Phys Rev Lett*, 118(4):048101, 2017.

[2] JR Blundell and EM Terentjev. Stretching semiflexible filaments and their networks. *Macromolecules*, 42(14):5388–5394, 2009.

[3] Masao Doi and Samuel Frederick Edwards. *The theory of polymer dynamics*, volume 73. Oxford University Press, 1988.

[4] Jorge M Ferrer, Hyungsuk Lee, Jiong Chen, Benjamin Pelz, Fumihiko Nakamura, Roger D Kamm, and Matthew J Lang. Measuring molecular rupture forces between single actin filaments and actin-binding proteins. *Proc Natl Acad Sci U S A*, 105(27):9221–9226, 2008.

[5] C Guzman, S Jeney, L Kreplak, S Kasas, AJ Kulik, U Aebi, and L Forro. Exploring the mechanical properties of single vimentin intermediate filaments by atomic force microscopy. *J Mol Biol*, 360(3):623–630, 2006.

[6] Gerhard A Holzapfel and Ray W Ogden. Elasticity of biopolymer filaments. *Acta Biomater*, 9(7):7320–7325, 2013.

[7] Jiliang Hu, Somaye Jafari, Yulong Han, Alan J Grodzinsky, Shengqiang Cai, and Ming Guo. Size-and speed-dependent mechanical behavior in living mammalian cytoplasm. *Proc Natl Acad Sci U S A*, 114(36):9529–9534, 2017.

[8] Fanlong Meng and Eugene M Terentjev. Theory of semiflexible filaments and networks. *Polymers*, 9(2):52, 2017.

[9] Raymond W Ogden. *Non-linear elastic deformations*. Courier Corporation, 1997.

[10] Zhao Qin, Laurent Kreplak, and Markus J Buehler. Hierarchical structure controls nanomechanical properties of vimentin intermediate filaments. *PLoS One*, 4(10):e7294, 2009.

[11] Cornelis Storm, Jennifer J Pastore, Fred C MacKintosh, Tom C Lubensky, and Paul A Janmey. Nonlinear elasticity in biological gels. *Nature*, 435(7039):191–194, 2005.

[12] Che Sun. Explicit equations to transform from cartesian to elliptic coordinates. *Mathematical Modelling and Applications*, 2(4):43–46, 2017.

[13] Yuri Tsuda, Hironori Yasutake, Akihiko Ishijima, and Toshio Yanagida. Torsional rigidity of single actin filaments and actin–actin bond breaking force under torsion measured directly by in vitro micromanipulation. *Proc Natl Acad Sci U S A*, 93(23):12937–12942, 1996.